ORIGINAL RESEARCH

Effects of bentonite on physical, mechanical and barrier properties of cellulose nanofibril hybrid films for packaging applications

Michelle Zheng · Mehdi Tajvidi · Ali H. Tayeb · Nicole M. Stark

Abstract There is an increasing attention to cellulose nanofibrils (CNFs) for food packaging applications due to their abundance, biodegradability, and low gas permeability. In this work, oxygen and water barrier performance is studied for bio-nanocomposite films formed by incorporation of two types of bentonite (PGN and PGV) at different loads (15, 30 and 45 wt%) into continuous CNF matrix. The resulting hybrid films were analyzed for their morphology, surface energy, mechanical strengths as well as water/oxygen barrier qualities. Both types of bentonite lowered the CNF degradation temperature and strength to some degree for reasons not so clear but perhaps due to partial disruption of the CNF H-bond network. It was revealed from microscopic study that clay particles form a layer within cellulose chains, resulting in alteration of composite structure. The contact angle analysis by polar and nonpolar liquids, suggested the PGN-containing samples were more hydrophilic; clay induced polar functionalities to the composite. While 15% PGN load reduced the water vapor transmission rate from 425 to 375 g/m^2 day, higher proportions of bentonite negatively affected this trend. Also, analysis of oxygen transmission rate showed the PGN effectively restricted the oxygen passage in dry state and to a lower extent at higher relative humidity. In WVTR analysis, PGN showed a superior performance over PGV attributable to its crystalline structure as evident in XRD patterns. The proposed hybrid CNF-BNT films in this study can present an eco-friendly alternative in packaging materials, especially where penetration of water vapor and oxygen is to be avoided.

M. Zheng
University of Southern California, Los Angeles, CA 90089, USA
e-mail: zhengmic@usc.edu

M. Tajvidi (✉)
School of Forest Resources and Advanced Structures and Composites Center, University of Maine, 117 Nutting Hall, Orono, ME 04469, USA
e-mail: mehdi.tajvidi@maine.edu

A. H. Tayeb
School of Forest Resources and Advanced Structures and Composites Center, University of Maine, 113 Nutting Hall, Orono, ME 04469, USA
e-mail: ali.tayeb@maine.edu

N. M. Stark
USDA Forest Products Laboratory, One Gifford Pinchot Drive, Madison, WI 53705, USA
e-mail: nstark@fs.fed.us

Graphical abstract
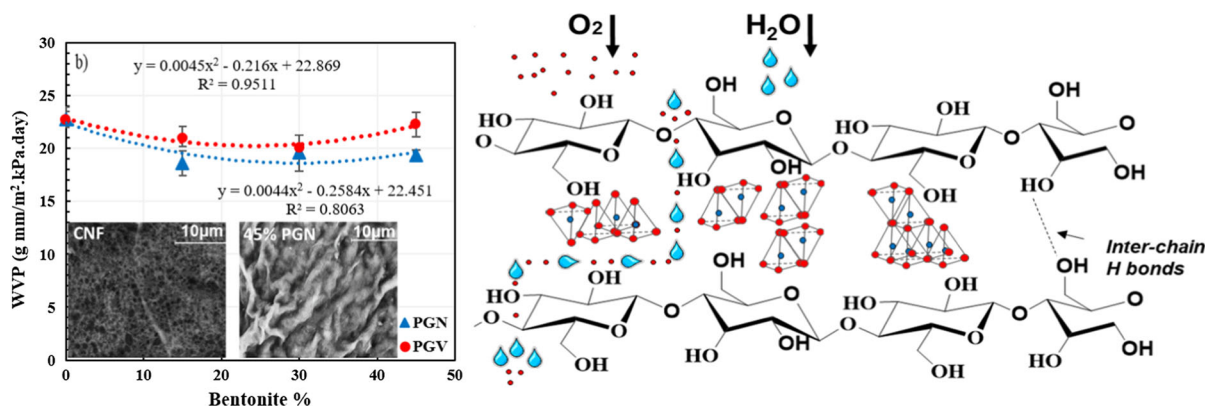
Abbreviations

CNFs	Cellulose nanofibrils
DCC	Dicarboxylic acid cellulose nanofibers
TGA	Thermogravimetric analysis
SEM	Scanning electron microscope
AFM	Atomic force microscope
WVTR	Water vapor transmission rate
WVP	Water vapor permeability
OTR	Oxygen transmission rate

Introduction

For long, synthetic petroleum-based plastics have been used for packaging applications, for their flexibility and barrier properties against gases and chemicals. However, owing to concerns over their disposal and long-term negative impacts on the environment, materials from renewable resources have been advocated as potential substitutes. Among the renewable polymers, cellulose is the most abundant organic material that constitutes about 1 trillion of world's annual biomass production (Klemm et al. 2005). Recently, utilization of nanocellulose-based materials has garnered increasing attention in food packaging industry, not only for their sustainability but also due to their excellent properties such as flexibility, high tensile/Young's modulus, unique rheology, low density, binding ability and high barrier against gases (Siró and Plackett 2010; Eichhorn et al. 2010; Klemm et al. 2011; Moon et al. 2011; Dufresne 2012; Hubbe et al. 2017; Wang et al. 2018; Tayeb et al. 2018; Noonan et al. 2019). Cellulose nanofibrils (CNFs) are liberated from stacked fibrils (delignified pulp is used as starting material) through vigorous mechanical fibrillation (Dufresne 2012), and can form strong biocomposites through a network of hydrogen bonds (Sehaqui et al. 2010, 2012). This concept is comparable to conventional paper making refining in which the fibrillation process improves the paper internal integrity (Tayeb et al. 2012). Furthermore, under low humidity, such a network possesses high barrier quality against oxygen. This, however may not be the case for water permeability, owing to the hydrophilic nature of cellulose (Fukuzumi et al. 2009; Kumar et al. 2014).

Among different approaches, recently the incorporation of nano-clay (unmodified and exfoliated) into nano-cellulosic matrix has been proposed to address this issue (Liu et al. 2011; Wu et al. 2012; Liu and Berglund 2012; Rhim et al. 2013; Gamelas and Ferraz 2015; Garusinghe et al. 2018). It is revealed that the high in-plane strength clay platelets can positively affect the mechanical and barrier properties of CNF-based membranes (Priolo et al. 2010; Yilmaz et al. 2012). In a study by Liu et al. (2011), clay-containing nanopapers were made with nanofibrillated cellulose (NFC) and sodium montmorillonite, under different mixing ratios (1:1–1:8). It was observed that lower level of clay (1:1) in dried films, leads to oxygen transmission rate (OTR) of 0.001 (cm^3

mm m^{-2} day^{-1} atm^{-1}), which is less than that of synthetic polymers. Although this trend was not evident in higher relative humidity, the produced nanopapers displayed adequate flexibility and high tensile strength. Also, hybrid films from dicarboxylic acid cellulose nanofibers (DCCs) and up to 25% talc (talc is a clay mineral) demonstrated diminished moisture absorption which was attributed to fundamental alteration in the film's network and talc's role in filling the gaps within the entangled fibrous structure (Liimatainen et al. 2013). Likewise, (Perotti et al. 2011), employed small particles of laponite clay to fill the gaps in a bacterial cellulose and similar concept was reported in the case of protein settlement in void spaces of the cellulosic network (Tayeb et al. 2017). It is known that in an aqueous system, exfoliated clay particles occupy the pores between the fibers and serve as blockade layers. The resulting structure contains highly tortuous diffusion paths that can hinder gas passage (Gusev and Lusti 2001). In addition, bentonite may prompt positive synergistic effects on the CNFs elastic and flexural modulus that would be useful for packaging materials. Nevertheless, in higher-level usage, agglomeration of excessive clay may interfere with the network of hydrogen bonds between the cellulose chains, causing a limit, beyond which, the mechanical properties may decrease (Spence et al. 2011). Therefore there is a need to understand how clay-type additives, once well distributed in the CNFs matrix, can affect its constitution, to obtain the desired barrier properties without a significant reduction in stiffness (Gabr et al. 2013).

In current work, hybrid CNF films with different bentonite contents, were studied for their barrier potential against gas and water transmission. Hypothetically, such system can form a less porous matrix due to layering effect of clay on the nano-structure (Fig. 1), which can effectively slow down the passage of oxygen, and to lesser extent, water molecules. Here we report on the inclusion of two commercial types of nanoclay, PGN and PGV, into CNF thin films to further delineate the role of each type in preparing a bio-based barrier layer against water and oxygen molecules. In addition, we investigated their synergistic effects on films surface free energy, internal integrity as well as the morphology of such interconnected system. Different characterization techniques such as water/oxygen permeability, microscopic evaluations, surface energy estimation, and tensile analysis, were employed to assess the morphology, mechanical and barrier performance of the films. Overall, the obtained data indicate promising prospects for the adoption of ecofriendly CNF-based films for utilization in drug or food packaging industries.

Materials and methods

Materials

Two types of bentonite, PGN and PGV, products of Nanocor, Hoffman Estates, IL were supplied by Minerals Technologies Inc., NY, USA, with the cation-exchange capacity (CEC) of 1.2 and 1.45 meq g^{-1} and moisture content of 12 and 18%, respectively. The letters P and G in the names stand for Polymer Grade. The platelet aspect ratios were 300–500 for PGN and 150–200 for PGV according to the manufacturer. They were exfoliated into 5.0 wt% suspensions using a sonicator (Branson 450 Sonifier, Ultrasonics Corporation, Danbury, CT) at 80% amplitude. A 1.0 wt% clay dispersion was

Fig. 1 Schematic of hypothetical insertion of bentonite particles within cellulose network to induce a tortuous diffusion path and improve water/gas barrier performance
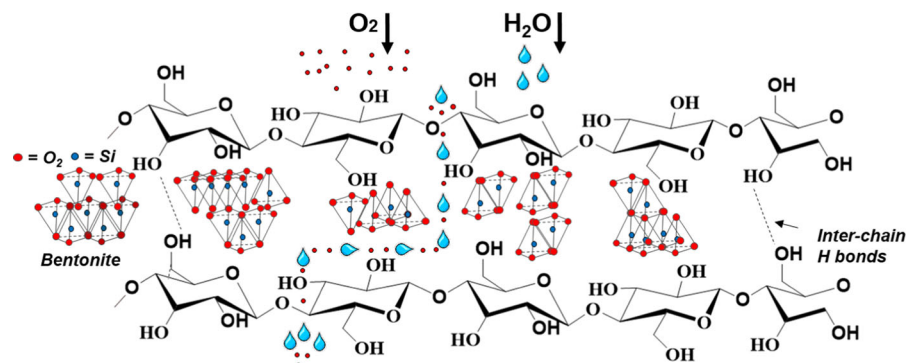
prepared by adding 1 g bentonite to 100 mL distilled water under vigorous mixing. CNF suspension with 3 wt% solids content, was supplied from the University of Maine's Process Development Center and diluted to 1 wt%. This CNF (with 20–50 nm in width and length of several microns), was solely produced through vigorous mechanical refining of bleached softwood pulp. A Moisture analyzer (Ohaus MB45 Corporation, Parsippany, NJ) was used to confirm the CNF solid content upon receipt.

Preparation of hybrid films

The 5 wt% solution of exfoliated bentonite was mixed with 1 wt% CNF suspension to varying clay weight percentages; 0% (control), 15%, 30%, and 45%. A planetary centrifugal mixer (Thinky 310, Thinky Corporation, Tokyo, Japan) was used to intermix them together for 1 min at 2000 rpm. De-foaming was carried out for 45 s at 2200 rpm. The final mixture (1% solid content) was poured into a 100×15 mm petri dish to the total solid weight of 0.35 g and samples were placed on a level surface under the hood to be air dried overnight.

Film characterization

Several methods were used to evaluate the films physical and mechanical properties with regards to what features they should possess if they were to be used for packaging purposes.

Surface free energy

Contact angle and surface free energy analysis were performed on both sides of the films by a Krüss mobile surface analyzer (Krüss GmbH, Hamburg, Germany) in which contact angles of double sessile drops for water and diiodomethane were measured. The surface free energy was calculated via the Advance software accompanying the instrument.

X-ray diffraction (XRD)

X-ray diffractometry was used to analyze the crystalline structure of raw materials and study the clay intercalation in hybrid films. X-ray patterns were obtained using a PANalytical X Pert Pro X-ray Diffractometer with a nickel filtered Cu–Kα radiation

source (λ = 1.54 Å) operating at 45 kV and 40 mA. 2θ values (from 5° to 65°) with a step size of 0.05°. Crystallinity index for CNF was evaluated using "Segal" equation (Segal et al. 1959):

$$CrI = \left(\frac{I_{cr} - I_{am}}{I_{cr}} \right) \times 100 \qquad (1)$$

where I_{am} is the lowest intensity scattered from the amorphous regions (2θ = 18°–19°) and I_{cr} is the highest intensity associated with the cellulose lattice diffraction (2θ = 22°–23°).

With respect to nanoclays, the crystalline structure of PGN and PGV were alike (Fig. 2), however peaks at 21.9° and 26.5° were only observed in PGN spectrum corresponding to the quartz usually found in clays (Vilela et al. 2007).

Thermoravimetric analysis (TGA)

The thermogravimetric analysis was conducted by a TGA Q500 (TA Instruments, New Castle, DE) on samples weighing between 2 and 10 mg. Heating was performed under nitrogen atmosphere, from room temperature to 600 °C at 10 °C/min with a flow rate of 40 mL/min. Cooling period was 10 min using a flow rate of 60 mL/min. Also, a few drops of 5 wt% bentonite solution were placed into a TGA pan and dried using Ohaus moisture analyzer (MB45, Ohaus
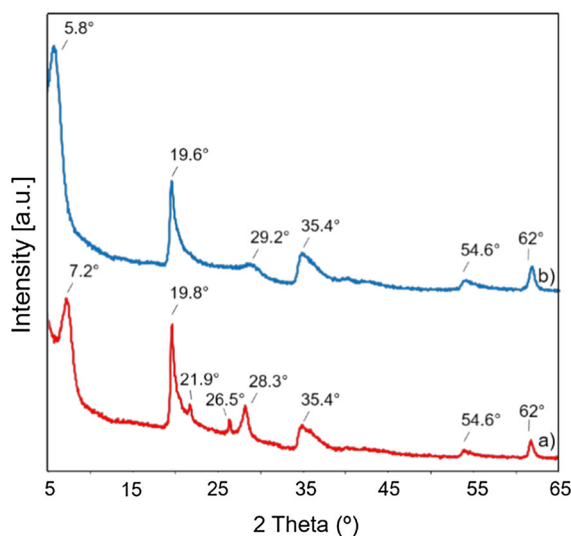

Fig. 2 X-ray diffraction patterns (2θ values from 5° to 65°) of **a** PGN **b** PGV powder

Corporation, Parsippany, NJ), for the subsequent thermogravimetric analysis.

Tensile testing

Tensile testing was carried out by a dynamic mechanical analysis (DMA) instrument (DMA Q800, TA Instruments, New Castle, DE). Films were cut into 3 mm width strips and the density of each specimen was determined. The maximum applied force was 18 N at a rate of 3 N/min and the corresponding Young's modulus, tensile strength, and strain at break were calculated from the obtained stress–strain curves. At least nine specimens were tested for each formulation.

Scanning electron microscopy

Films surface structure was observed by a Hitachi TM 3000 SEM; images were taken of both sides at various magnifications. Cross-sections of the broken films (used in tensile measurements) were also analyzed. Additionally, several drops of exfoliated bentonite particles, in dilute solution, were placed on a piece of a glass coverslip and were scanned after being dried. ImageJ image analysis software (NIH, Bethesda, MD) was used to analyze the particle size at 2000× magnification.

Atomic force microscopy

A Nanomagnetics Instruments ezAFM (Nanomagnetics Instruments Oxford, UK) was employed to evaluate the roughness and morphology of the films. For each film, 10 × 10 μm topographic images of both sides were collected to measure the roughness on an approximately $(570,000)^2$ pixel sized area. The resulting data was used to scrutinize the level of bentonite exfoliation.

Water vapor transmission

Gravimetric technique was used to characterize the water vapor barrier property of the films according to standard method (ASTM E96/E96M-16). Briefly, each film was cut into a circle (65 mm in diameter) and the area was calculated. Glass jars were filled with 25 mL distilled water and circular-cut films were fitted on top of the jars (same direction that were air dried),

tightly sealed by a silicon rubber, and weighed before being left in standard conditioned room (23 °C, 50% RH) for 24 h. In the end, they were weighed again and water vapor transfer rate (WVTR) and water vapor permeability (WVP) values were calculated using Eqs. (2) and (3).:

$$\mathrm{WVTR}\left(\frac{\mathrm{g}}{\mathrm{m}^2}\right) \mathrm{day} = \frac{\Delta_{mass}}{(r^2).\pi.\mathrm{day}} \tag{2}$$

where Δ_{mass} is the difference between the mass of the jar before and after the test and r is the radius of the film. The water vapor permeability (WVP) was calculated using Eq. (2), (Bedane et al. 2015) to reflect the films varying thickness.

$$\mathrm{WVP}\left(\frac{\mathrm{g\,mm}}{\mathrm{day\,kPa\,m^2}}\right) = \mathrm{WVTR}.\frac{thickness}{P_{(Sat)}.\Delta RH\%} \times 100 \tag{3}$$

where $P_{(sat)}$ represents the water vapor saturation pressure at the experiment temperature (2.81 kPa–23 °C). ΔRH is the difference of the relative humidity between inside and outside the container.

Oxygen transmission rate

Oxygen transmission rate (OTR) was measured according to the procedure outlined in (ASTM D3985-17) using an oxygen transmission rate test system (Ox-Tran Module 2/22, Mocon, Inc.,). Rezero cycles were performed after every two tests for 30 min. The permeant (O_2) concentration was 100%. The permeation area of the samples was masked to 5.0 cm^2 and the OTR was determined for three sequential exposures, 23 °C and 0% RH, 23 °C and 50% RH, and 23 °C and 90% RH. The exposures were the same for both the test gas and the carrier gas.

Statistical analysis

All data were statistically analyzed in a completely randomized design using analysis of variance (ANOVA). Means were grouped using Duncan's Multiple Range Test (DMRT) and the comparisons were made at the 95% confidence level.

Results and discussion

Hybrid films characterization

While the particle distribution in both groups of clays were inclined towards the smaller size (Fig. 3), the PGV possessed slightly larger ferret's diameters. This suggests that the PGV may be less prone to agglomeration and/or more difficult to be exfoliated. This is in agreement with poor stability of PGV suspension in water, and its tendency to settle out once left unstirred.

According to the product datasheet, the PGN has higher aspect ratio and potentially can form a better structure within the CNF film. Also, PGN demonstrates lower moisture content and cation-exchange capacity, which would make it difficult for water molecules to travel through the films. Bentonite films yielded roughness values within the micrometers scale as was expected. Some variations in data was seen due to clay agglomeration and uneven drying of the droplets on the glass surface. The average surface roughness of PGN and PGV droplets on glass slide were 0.27 and 0.31 μm with root mean square (RMS) values of 0.32 and 0.35 μm, respectively.

CNF and bentonite crystalline structure were analyzed by the X-ray diffractograms (Fig. 4). All CNF samples had peaks at 16° (1–10 and 110 combined) and 22.7° (200) which are the characteristic of the cellulose (I) (Buschle-Diller and Zeronian 1992; French 2014). The crystalline index (CrI) in the
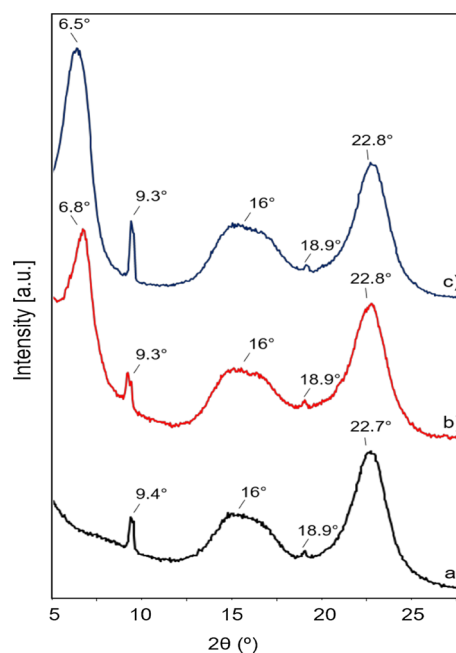

Fig. 4 X-ray diffraction patterns of (a) reference CNF, (b) CNF-15%PGN, (c) CNF-15%PGV

reference CNF films was determined as 59% based on the method developed by (Segal et al. 1959).

Compared to the CNF, no change was observed in clay-added films, except for a new signal at 6.5° which is associated to the primary diffraction of the clay's silicates showing the trace of bentonite in the hybrid films (Yermiyahu et al. 2005; Liu and Berglund 2012). Also, most of the clay peaks observed in Fig. 2, (2θ = 15°–25°) were not detected in the clay-
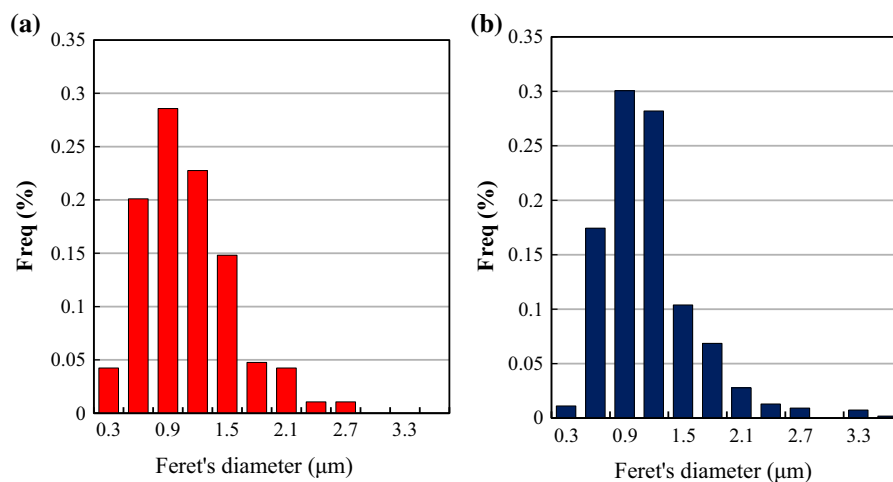

Fig. 3 Histogram of ferret's diameter distribution for bentonite particles, **a** PGN and **b** PGV

containing films which can be due to their weak intensity and overlap with CNF peaks. The observed peaks at 9.4° and 18.9° are not related to any crystalline domain in the cellulose, but perhaps implies the presence of some unidentified impurities in the CNF samples.

To determine the effect of bentonite on CNF film thermal stability, thermogravimetric tests were performed from 25 to 600 °C. Films containing both types of clays showed minimal degradation over the entire temperature range, indicating that the observed weight loss was mostly due to cellulose breakdown. Additionally, the amount of residue left after 600 °C increased linearly with bentonite content, indicating clay's minimal degradation. However, as shown (Fig. 5a, b), the 45% PGV content resulted in relatively lower residue.

As shown in the derivative TGA (Fig. 5a-1, b-1), the degradation temperature decreased with the addition of both types of clays, however this effect was more clear in PGV-containing hybrids. The 45% PGV-containing composites decomposed over a wider range of temperature, (small peak at 250 °C and the intense peak at 300 °C) that was not seen for CNF. This clearly indicates the alteration in films decomposition behavior owing to the presence of bentonite. Table 1, summarizes the thermogravimetric analysis results. As shown, the incorporation of bentonite generally decreased the films degradation temperature, and increased the residue content. The reduction in degradation temperature was more significant for PGV (up to 15%), however this trend was less noticed once using higher clay loads (up to 45%). Compared to PGV, PGN showed a less initial weight loss. More
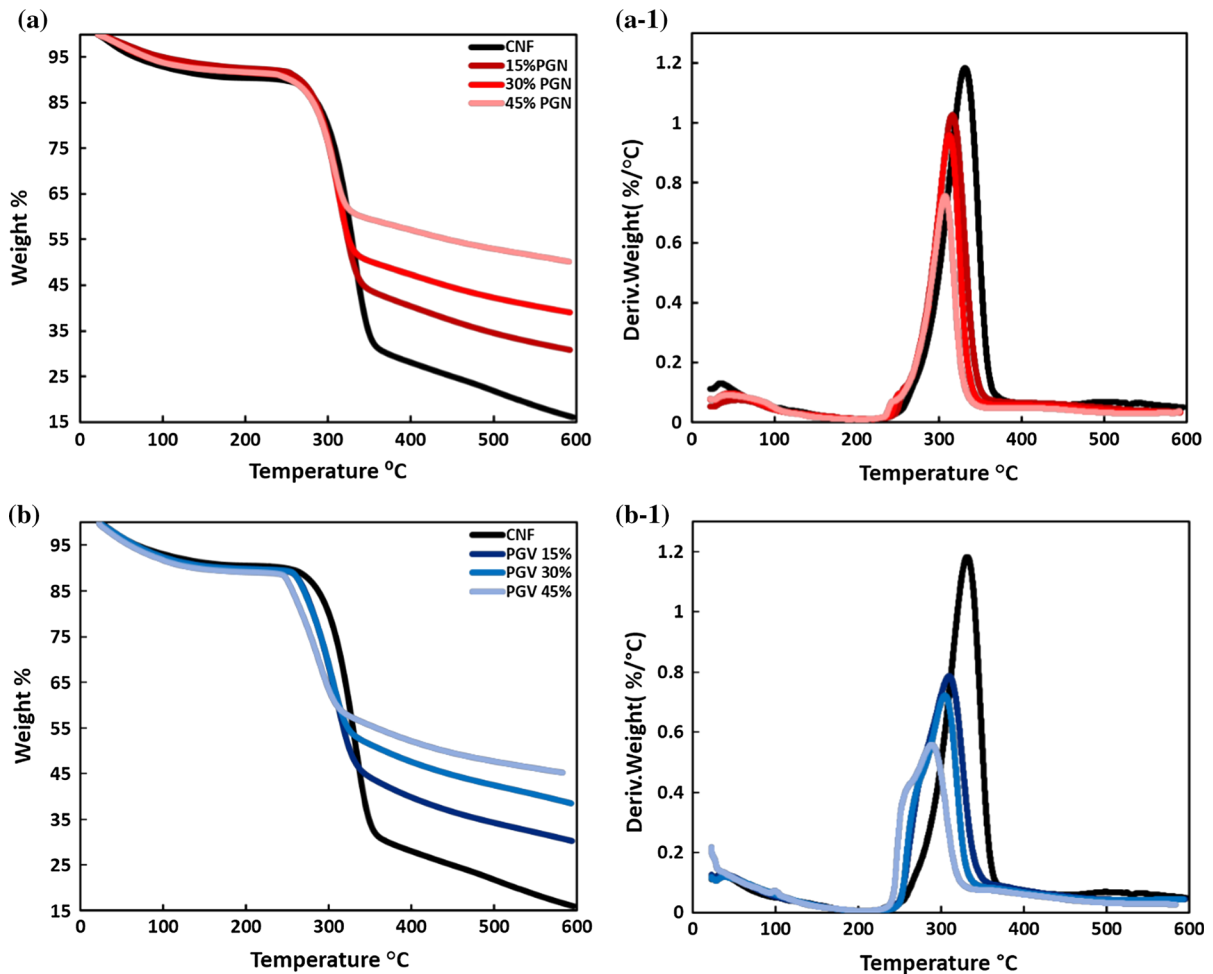

Fig. 5 TGA thermograms of **a** CNF and **b** bentonite-CNF nanocomposites. **a-1**, **b-1** are the corresponding DTG curves

Table 1 Thermal stability results of CNF-bentonite films (ramp from 25 °C to 600 °C at 10 °C/min) MC: moisture content, T (°C): temperature

	MC (wt%)	T at 10% mass loss	T at 50% mass loss	Onset of degradation	Max of degradation	Residue at 600 °C (wt%)
Neat CNF	8.7 ± 1.0	295.6 ± 1.9	335.7 ± 2.2	281.2 ± 3.2	329.4 ± 3.0	14.8 ± 4.0
15% PGN	8.7 ± 1.4	292.6 ± 1.8	339.7 ± 3.2	274.5 ± 1.0	318.3 ± 2.4	34.2 ± 1.3
30% PGN	8.5 ± 1.0	292.2 ± 1.1	435.8 ± 5.0	274.8 ± 1.9	315.1 ± 0.7	43.2 ± 0.7
45% PGN[a]	8.4 ± 0.004	293.8 ± 0.8	–	268.6 ± 1.2	311.2 ± 0.5	54.9 ± 0.4
15% PGV	9.8 ± 0.5	282.7 ± 1.6	346.2 ± 0.2	253.9 ± 1.6	311.6 ± 0.8	33.4 ± 0.3
30% PGV	10.2 ± 0.01	281.5 ± 1.2	450.8 ± 4.3	254.7 ± 0.8	307.1 ± 0.5	42.8 ± 0.04
45% PGV[a]	11.1 ± 0.3	280.8 ± 1.7	–	254.6 ± 0.8	302.0 ± 0.2	50.3 ± 0.5

[a]Samples did not lose 50% mass and no data was collected

remaining residue was seen at higher bentonite level (as measured at 600 °C under pyrolysis condition), that can be due to bentonite's thermal stability and hence minimal degradation.

Generally it is expected that incorporation of nano-clay into CNF film retard the degradation process due to the formation of silicate layers as a protective barrier and/or via inducing a torturous path delaying the volatilization of volatile products (Leszczyńska et al. 2007). However, the observed marginal increase in the decomposition rate may have raised from the stacked silicate layers that can store the accumulated heat and introduce an energy source accelerating the degradation process. This phenomenon was reported in the work by other authors (Sinha Ray and Bousmina 2005; Zhou and Xanthos 2009).

Tensile properties

Young's modulus analysis (date not shown) confirmed the reduction in films' modulus by adding PGN up to 30% (no significant decrease was seen for 45% PGV). However, the corresponding normalized data, according to their densities, showed either no significant change compared to the CNF, or a slight increase (Fig. 6a).

Duncan's multiple range test was performed to analyze the normalized data for tensile strength at break. While PGN introduction reduced the films' strength, addition of PGV had no promising effect. Similar trend was observed for the strain at break values (Fig. 6c). Overall, while higher concentrations of PGV (30% and 45%), gave rise to strain at break, PGN caused the same effect at a lower load (15%).

Area under the curve, which is referred to as toughness, can be obtained by integrating the area under stress–strain curve. It reflects the absorbed energy of mechanical deformation per unit volume before fracture. As evident (Fig. 6d), both types of clay had a reducing effect on toughness values. Finally, the tensile testing indicated a partial positive role of PGV clay on films mechanical properties, only at 15% load. Higher bentonite led to a poorer mechanical properties (Fig. 6b).

Surface and cross-sectional morphology of hybrid films

The cross-sections of all fractured samples from tensile tests were analyzed by SEM (Fig. 7). As shown, PGN-containing films had a more ductile rupture, as the structure pulled apart, but PGV films demonstrated more of cracking phenomenon, an evidence for a more brittle break. The reason for this dissimilarity is not fully known but it can be related to the difference in clays structures.
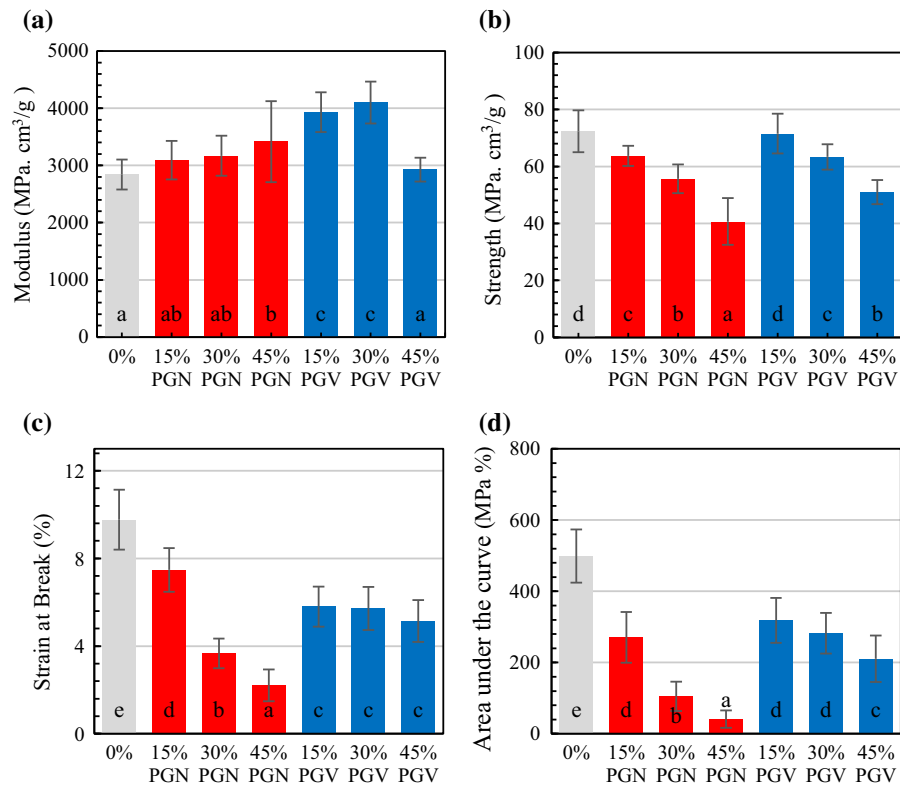
(a)

(b)

(c)

(d)

Fig. 6 Films' Young's Modulus **a** strength at break **b** (**a**, **b** are normalized according to the films density), strain at break (**c**) and area under the curve (**d**). Data organized into letter-marked groups by Duncan's tests and based on 95% level of confidence. Columns with common letters did not have significant difference at 95% confidence level

This difference in rupture quality is in line with what was observed in tensile data presented in Fig. 6. Ductile materials usually withstand more strain and have lower modulus, whereas brittle formations behave in an opposite manner. The normalized modulus data indicated that the 15% and 30% PGN samples possessed lower modulus than their corresponding PGV films, point out to their ductile and brittle structures, respectively. However the strain at break values only confirmed this trend for the 15% PGN and above this level films were brittle.

Surface characterization

Figure 8, shows SEM images of hybrid CNF films. As obvious, the porous structure in unmodified CNF film turned into a less permeable, layer-topped configuration upon the incorporation of bentonite particles.

A layer of bentonite was seen on the CNF matrices and this layering phenomenon was more distinguishable within samples of higher clay content, possibly due to bentonite ability to fill the spaces within interlocking CNF fibers. It is reported that flat, exfoliated bentonite platelets potentially can reduce the passage of gasses and liquids, such as water through this mechanism (Garusinghe et al. 2018).

Atomic force microscopy was used to evaluate the films roughness and their surface morphology. Data in Table 2 and Fig. 9 show that the tops roughness values remained unchanged, implicating no significant surface rearrangement. This might be owing to exposure to the air-flow during the drying. However, the bottom roughness tended to decrease proportionally with bentonite addition. In agreement with this, is the laboratory observations during the drying (data not presented) that confirmed more clay-containing films tended to stick better to the plastic petri dish which led to smoother surfaces.

Since any clay formula applied in the hybrids may influence the surface adhesion and wettability (as critical factors affecting the initial adsorption), nanostructures with different bentonite percentages were
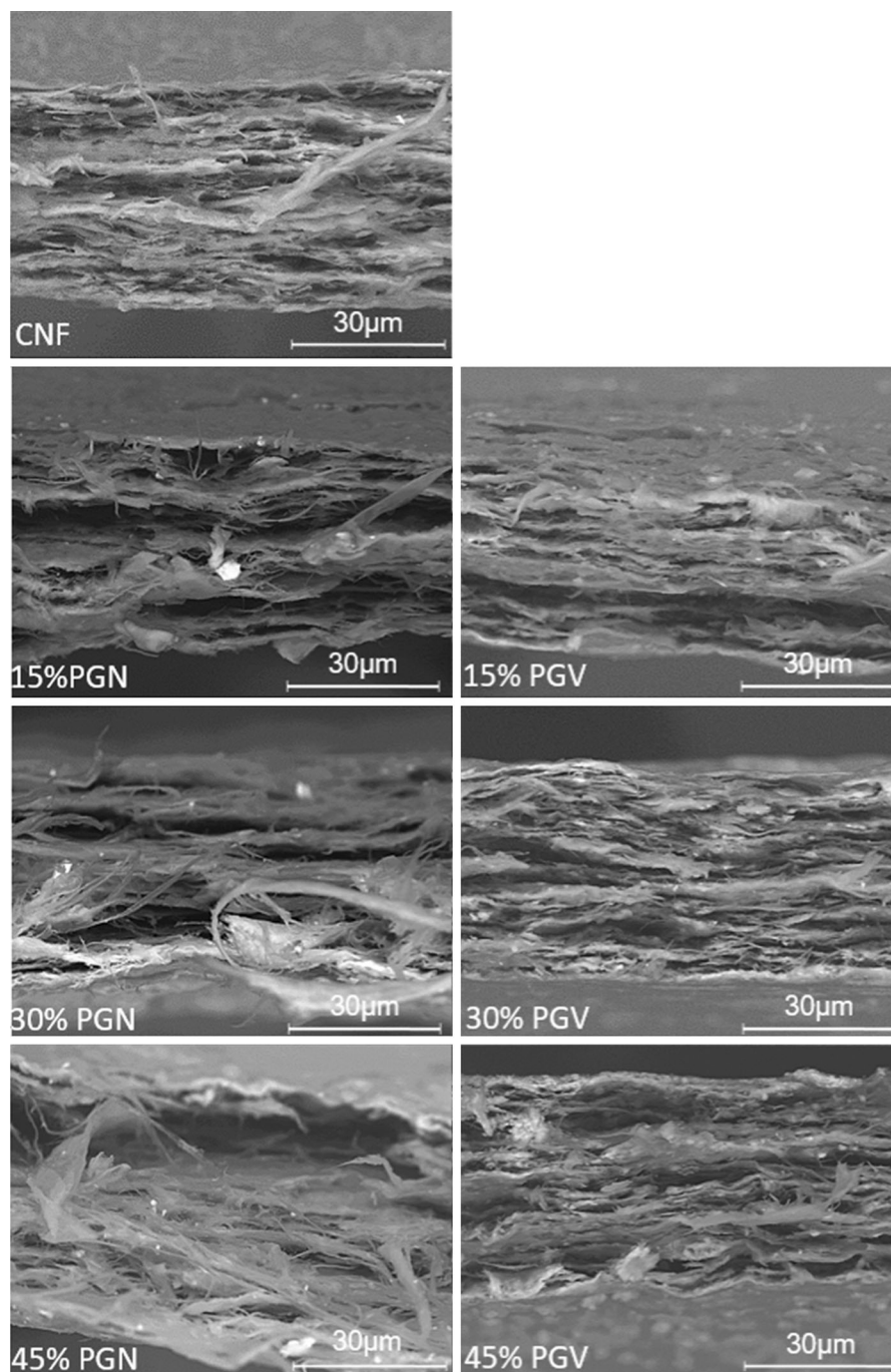
Fig. 7 2000× magnitude cross sectional SEM images of CNF-bentonite films after fracture in tensile tests

prepared and evaluated in terms of surface free energy. Contact angles were measured using water and diiodomethane on the top surfaces to monitor the change in films free energy. Six replicates were used for each surface and statistical analysis was carried out by Duncan's multiple range test following analysis of variance. As became clear (Fig. 10) all clay-carrying samples (excluding 15%PGV) had reduced water contact angles on top of the film, signaling to a higher hydrophilicity due to the clay presence. This trend,
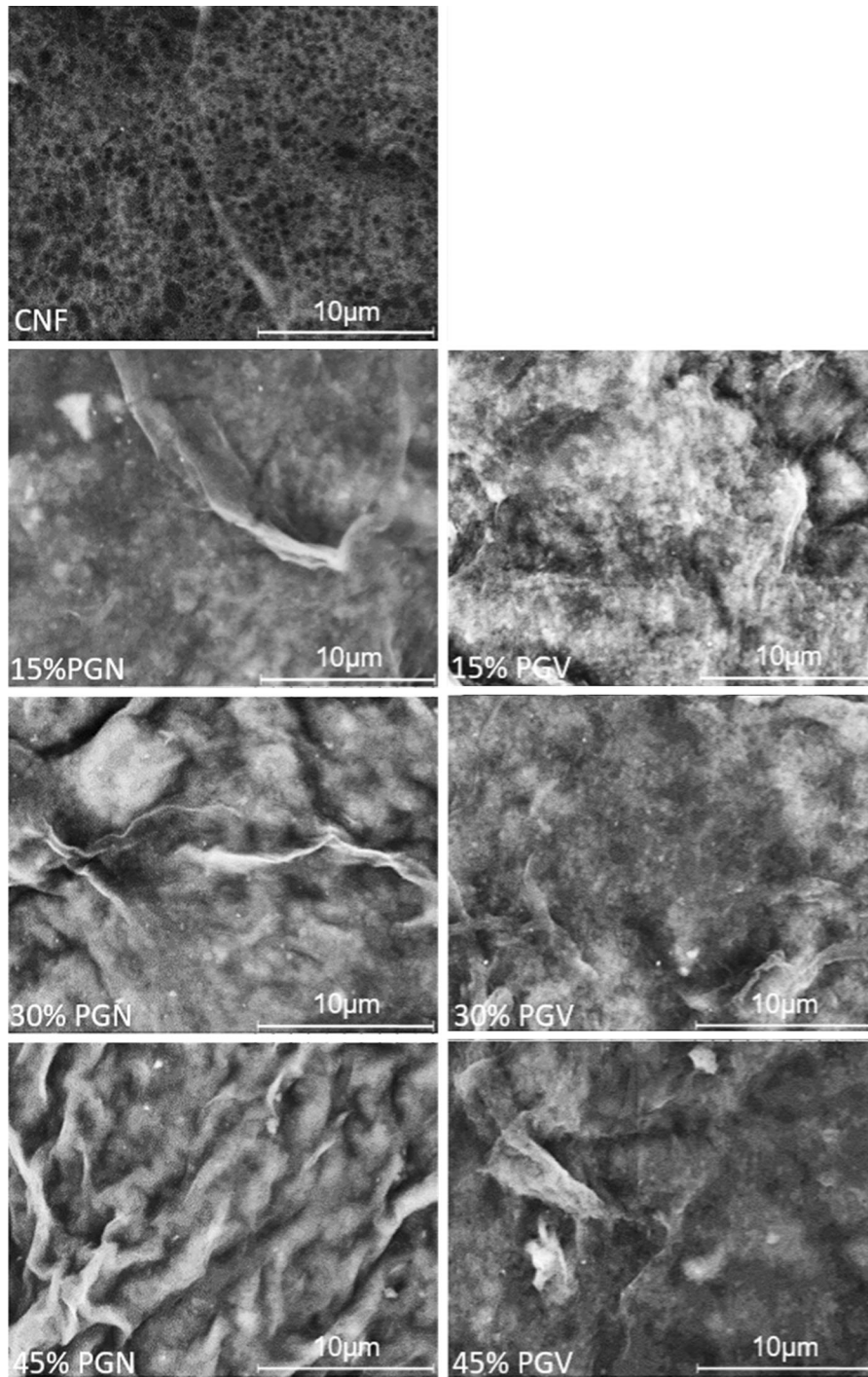
Fig. 8 SEM top surface images of CNF-bentonite films at 7000× magnitude

was more apparent for PGN, perhaps for its harder to exfoliate nature.

The surface free energy was calculated using the disperse index and polarity of the hybrid films and it became evident that the increase in surface energy

Table 2 Roughness data (µm scale), obtained from AFM analysis

Formulation	Bottom R_a	Bottom R_q	Top R_a	Top R_q
Neat CNF	0.42	0.49	0.48	0.57
15%-PGN	0.58	0.70	0.47	0.59
30%-PGN	0.21	0.26	0.42	0.50
45%-PGN	0.07	0.08	0.62	0.74
15%-PGV	0.51	0.63	0.49	0.59
30%-PGV	0.49	0.56	0.43	0.51
45%-PGV	0.17	0.21	0.48	0.60

values was mostly for the induced polarity by bentonite.

For the top surface, all PGN formulations and most of PGVs (30–45%), displayed a remarkable increase in the free energy which was mostly for the change in the polarity. The disperse index was fairly constant among the formulations based on Duncan's test. Also plotting the average contact angle versus roughness results, showed no correlation between roughness and surface free energy.

Water contact angle and surface free energy values point out to the higher hydrophilicity/polarity in clay-containing films which may not be desirable for hybrids' water/oxygen barrier features; a more water-loving structure can permit the absorption of water vapor and loosen the fiber–fiber bonds especially at elevated relative humidity (Fig. 11). However, this does not preclude the clay's function as a physical blockade within the nanofibril network.

Water vapor transmission and permeability

Three films from each batch were used for the water vapor permeability analysis. Figure 12 shows water vapor permeability (WVP) and water vapor transmission rate (WVTR) results. In the WVTR equation, it is only the available area in films that is used for calculations, but the more accurate WVP takes into account the factor of films thickness.

As shown in Fig. 12a, the 15% PGN is the only batch that reduced WVTR (from 425 to 375 g/m^2 day) and above this level, transmission rate was increased to 402 and 445 g/m^2 day, respectively. Almost the
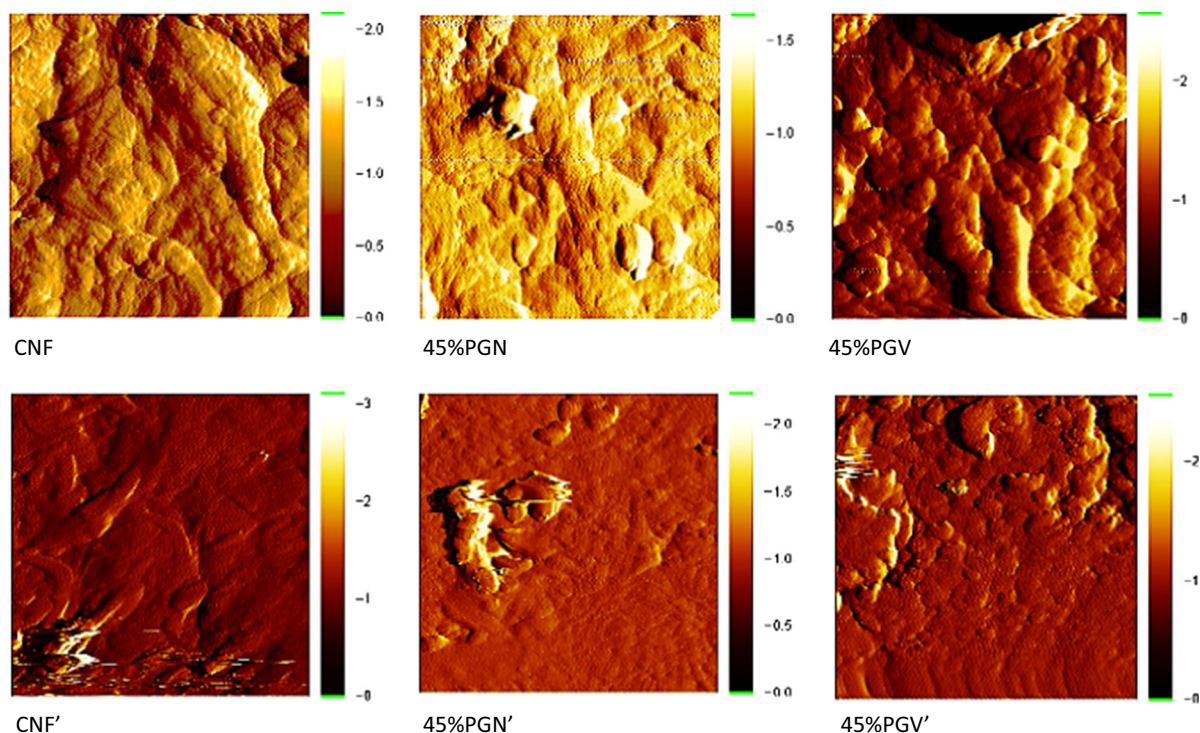

Fig. 9 AFM images of top (CNF, 45%-PGN, 45%-PGV) and bottom (CNF', 45%-PGN', 45%-PGV') surfaces of CNF-bentonite films. Image windows are 10 × 10 µ
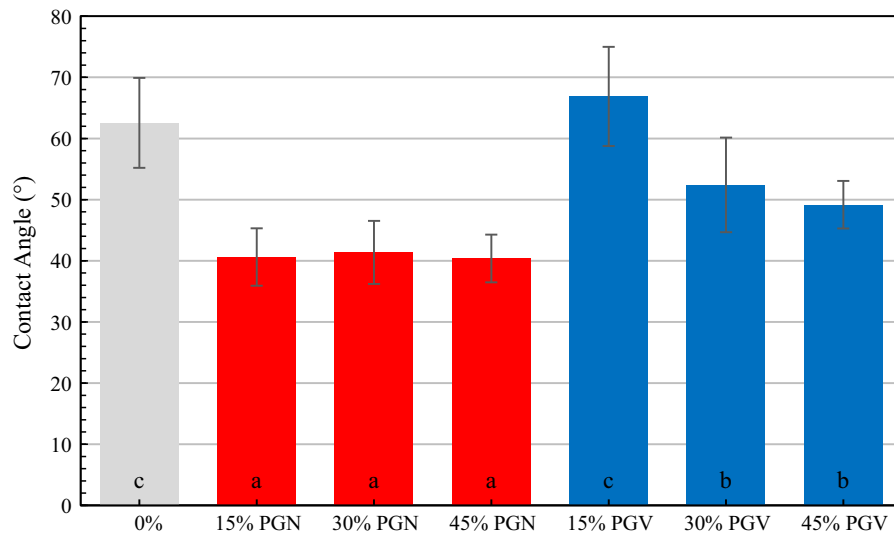
Fig. 10 Water contact angles for top of the films, letter-grouped, based on Duncan's test
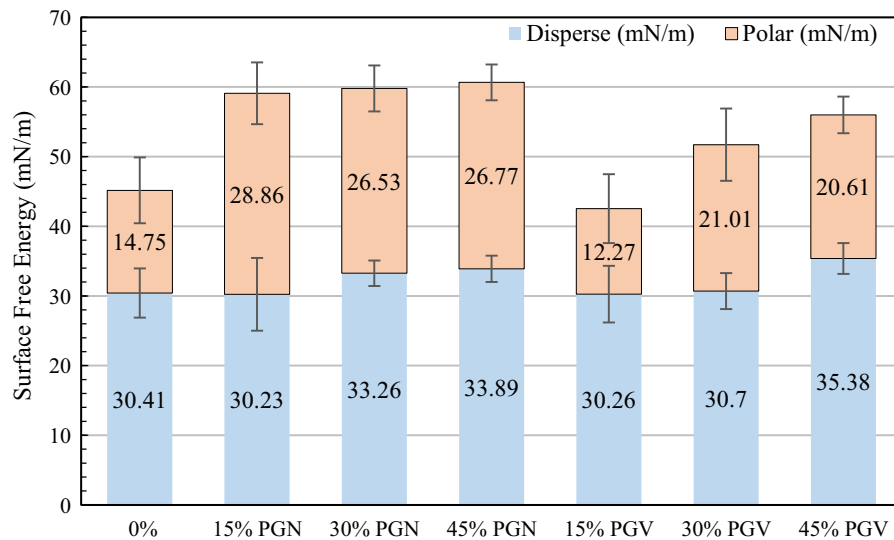

Fig. 11 Surface free energy distribution divided into disperse and polar portions for the top of CNF-bentonite films

same behavior was observed in WVP results which confirmed clay's positive contribution to CNF barrier property, only up to a certain point as was also reported in our recent study (Tayeb and Tajvidi 2018). Comparison between PGN and PGV performance suggests that PGN was a better additive for reducing water vapor permeability, though it increased the state of water affinity in the matrices that means the improvement in WVP was more related to the structural changes rather than alteration in films hydrophilicity. This can be related to its higher aspect

ratio, crystalline structure and ability to hinder the pores inside the cellulosic network. In a pertinent study, the clay particles were reported impermeable enough to force the water molecules to go around the platelets which led to a longer penetration path (Honorato et al. 2015).

Both types of studied clays, showed parabolic WVTR trends, meaning that excessive bentonite-load had an adverse effect because of clay agglomeration and its subsequent interference with hydrogen bonds in the CNF films. Thus, it is useful to look at bentonite
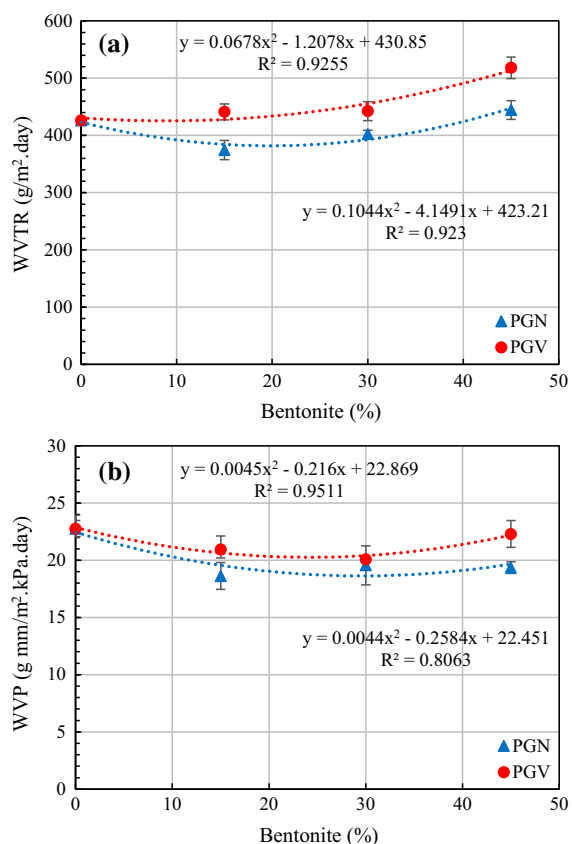
Fig. 12 Water vapor transmission rate (**a**) and water vapor permeability (**b**) scatter plots with quadratic trend lines

effect on such films at lower ratios in follow-up future studies.

Oxygen transmission rate

CNF films are known to be excellent barriers against oxygen due to their dense structure. Table 3 summarizes the oxygen transmission data for reference CNF and CNF-PGN hybrid films containing 15% clay. Coefficients of variation (C.V.%) are also presented. The obtained values for CNF films are in the same

range as already reported in the literature (Aulin et al. 2010, 2012; Kumar et al. 2014) and inclusion of PGN bentonite, induced even less oxygen transmission rate to the structure at lower relative humidity (0–50%). The formation of bentonite layers within the CNF film, reduced the oxygen permeability to a great extent which is attributable to a packed and more tortuous structure.

As reported in our study and in agreement with the literature, at higher humidity, these CNF-based matrices lost their gas barrier quality, even in the presence of clay. The effectiveness of PGN to reduce CNF OTR was considerably diminished a higher relative humidity; the addition of 15% PGN reduced OTR by 62%, 47% and 15% at relative humidity of 0%, 50% and 90%, respectively. Analysis of Variance (ANOVA) followed by Duncan's Multiple Range Test (DMRT) showed that the difference between the OTR of reference CNF and that of the 15%PGN formulation at all relative humidity levels was statistically significant at 95% confidence level. The effect of relative humidity on the increase of OTR was also found statistically significant in all cases expect between the OTR of CNF films at 0% and 50% relative humidity. One widely accepted scenario for the loss of OTR barrier properties is the swelling and plasticizing of nanofibrils at higher moisture contents which can effectively open the gas passage paths (Österberg et al. 2013).

Comparison of results with the literature

The underlying concept in this study was that the insertion of nano-scale minerals (i.e., bentonite) within the continuous film of CNF could prompt a defect-free structure with higher resistance to water vapor and oxygen penetration. This is particularly important in food packaging applications where the permeation of oxygen and water to the protective layer can cause deterioration of the food. While the

Table 3 OTR values for CNF and CNF-bentonite films (85/15 ratio); 0, 50 and 90 represent the corresponding relative humidity

Sample code	CNF	CNF	CNF	PGN	PGN	PGN
Humidity (%)	0	50	90	0	50	90
OTR (cm^3/m^2/day)	15.67	19.65	63.04	5.95	10.45	53.55
C.V.%	5.1	2.0	6.2	4.6	1.2	8.0

presented work owns a unique setting and aims an angle not found in the literature, the obtained results agree with the reported literature. For instance, in a study by Algar and col., a hybrid bio-nanocomposite that was fabricated through in situ assembly of bacterial cellulose (BC) and 7–13 wt% plate-shaped montmorillonite (MMT), showed a lower porosity than neat BC. They attributed this phenomenon to the presence of MMT that had imparted a tortuous diffusion path within the nanocellulose network. Moreover, the resulting film possessed a markedly higher water and oxygen barrier property by 70% and 80% respectively (Algar et al. 2016). In another work, a hybrid nacre-like structure of nanocellulose (NFC) and layered silicates (50 wt%) displayed a great strain-to-failure, fire retardancy and gas barrier quality (Liu et al. 2011). Likewise, Wu et al. adopted a similar theme but employed TEMPO oxidized nanocellulose in place of regular CNF. The TOCN film that contained various ratios of MMT, demonstrated excellent transparency and ultrahigh mechanical and gas barrier function. Thus, in light of the cited reports, it is conceivable that the combination of nanocellulose and clay-type additives can lead to exceptional features not seen in common bio-materials such as starch or poly lactic acid. However, despite the promises, one remaining challenge is the dependency of such systems on their interface properties (e.g., morphology, surface energy and charge) that necessitates the control of several parameters for the desired efficiency (Gamelas and Ferraz 2015). Besides, in most of the cases a vigorous mixing condition is suggested to avoid mediocre interface interaction and poor dispersion of either components (Rhim et al. 2013; Gamelas and Ferraz 2015).

Conclusions

We incorporated different ratios of exfoliated bentonite particles (PGN and PGV) in continuous CNF matrix (with random fibril orientation) to produce strong hybrid nanocomposites with lower water/oxygen barrier properties. Microscopic studies, revealed the formation of clay layers within the nanocellulose constitution that reduce the surface roughness. While PGN induced some ductility, introduction of PGV resulted in a brittle structure. As with the WVP, both types of bentonites caused a reduction in water permeability to a certain degree (promising ratios; 15–30% PGN), however excessive clay load adversely affected the barrier properties. Obtained results may be explained on the basis of filled non-connecting pores in CNF films. According to surface energy analysis, PGN introduced higher hydrophilicity to hybrid films compared to PGV, explaining their tendency to absorb more water at higher clay proportions. Also, TGA data confirmed a lower thermal degradation point, especially when PGN was used as an additive. The difference in two types of clays (both for moisture barrier properties and thermal degradation behavior) is not clear but perhaps can be related to the difference in their crystalline domains as evident in XRD findings. At 45% PGN by weight of bentonite, the highest modulus and lowest strength and strain at break were observed which indicates less flexibility in the films. The OTR analysis, confirmed a high oxygen barrier quality, which is required for food packaging applications. Clay-incorporated films (type PGN) had an OTR value of 5.95 ($cm^3/m^2/day$) at 0% humidity, which was almost three times lower than that of the reference CNF films. This affirms nano-clay's positive effect to further blockade the gas passage through the CNF structure. Overall, the obtained data, advocate the promising role of bentonite, once well distributed in CNF films, as an effective obstacle for water/oxygen penetration, despite a partial reduction in film mechanical properties. Such an environmentally safe bio-composite can potentially be applied for food packaging especially where barrier layers are needed for food preservation.

References

Algar I, Garcia-Astrain C, Gonzalez A et al (2016) Improved permeability properties for bacterial cellulose/montmorillonite hybrid bionanocomposite membranes by in-situ assembling. J Renew Mater 4:57–65. https://doi.org/10.7569/JRM.2015.634124

ASTM D3985–17 (2017) Standard test method for oxygen gas transmission rate through plastic film and sheeting using a coulometric sensor. ASTM International, West Conshohocken

ASTM E96, E96M–16 (2016) Standard test methods for water vapor transmission of materials. STM International, West Conshohocken

Aulin C, Gällstedt M, Lindström T (2010) Oxygen and oil barrier properties of microfibrillated cellulose films and coatings. Cellulose 17:559–574

Aulin C, Salazar-Alvarez G, Lindström T (2012) High strength, flexible and transparent nanofibrillated cellulose–nanoclay biohybrid films with tunable oxygen and water vapor permeability. Nanoscale 4:6622–6628

Bedane AH, Eić M, Farmahini-Farahani M, Xiao H (2015) Water vapor transport properties of regenerated cellulose and nanofibrillated cellulose films. J Memb Sci 493:46–57

Buschle-Diller G, Zeronian SH (1992) Enhancing the reactivity and strength of cotton fibers. J Appl Polym Sci 45:967–979. https://doi.org/10.1002/app.1992.070450604

Dufresne A (2012) Nanocellulose: from nature to high performance tailored materials. Walter de Gruyter GmbH & Co KG, Berlin

Eichhorn S, Dufresne A, Aranguren M et al (2010) Review: current international research into cellulose nanofibres and nanocomposites. J Mater Sci 45:1–33

French AD (2014) Idealized powder diffraction patterns for cellulose polymorphs. Cellulose 21:885–896. https://doi.org/10.1007/s10570-013-0030-4

Fukuzumi H, Saito T, Iwata T et al (2009) Transparent and high gas barrier films of cellulose nanofibers prepared by TEMPO-mediated oxidation. Biomacromolecules 10:162–165. https://doi.org/10.1021/bm801065u

Gabr MH, Phong NT, Abdelkareem MA et al (2013) Mechanical, thermal, and moisture absorption properties of nano-clay reinforced nano-cellulose biocomposites. Cellulose 20:819–826

Gamelas JAF, Ferraz E (2015) Composite films based on nanocellulose and nanoclay minerals as high strength materials with gas barrier capabilities: key points and challenges. BioResources 10:6310–6313. https://doi.org/10.15376/biores.10.4.6310-6313

Garusinghe UM, Varanasi S, Raghuwanshi VS et al (2018) Nanocellulose-montmorillonite composites of low water vapour permeability. Colloids Surf A Physicochem Eng Asp 540:233–241

Gusev AA, Lusti HR (2001) Rational design of nanocomposites for barrier applications. Adv Mater 13:1641–1643

Honorato C, Kumar V, Liu J et al (2015) Transparent nanocellulose-pigment composite films. J Mater Sci 50:7343–7352

Hubbe MA, Tayeb P, Joyce M et al (2017) Rheology of nanocellulose-rich aqueous suspensions: a review. BioResources 12:9556–9661

Klemm D, Heublein B, Fink H-P, Bohn A (2005) Cellulose: fascinating biopolymer and sustainable raw material. Angew Chemie Int Ed 44:3358–3393

Klemm D, Kramer F, Moritz S et al (2011) Nanocelluloses: a new family of nature-based materials. Angew Chem Int Ed 50:5438–5466

Kumar V, Bollström R, Yang A et al (2014) Comparison of nano- and microfibrillated cellulose films. Cellulose 21:3443–3456

Leszczyńska A, Njuguna J, Pielichowski K, Banerjee JR (2007) Polymer/montmorillonite nanocomposites with improved thermal properties: part II. Thermal stability of montmorillonite nanocomposites based on different polymeric matrixes. Thermochim Acta 454:1–22. https://doi.org/10.1016/J.TCA.2006.11.003

Liimatainen H, Ezekiel N, Sliz R et al (2013) High-strength nanocellulose-talc hybrid barrier films. ACS Appl Mater Interfaces 5:13412–13418. https://doi.org/10.1021/am4043273

Liu A, Berglund LA (2012) Clay nanopaper composites of nacre-like structure based on montmorrilonite and cellulose nanofibers—improvements due to chitosan addition. Carbohydr Polym 87:53–60. https://doi.org/10.1016/j.carbpol.2011.07.019

Liu A, Walther A, Ikkala O et al (2011) Clay nanopaper with tough cellulose nanofiber matrix for fire retardancy and gas barrier functions. Biomacromolecules 12:633–641

Moon RJ, Martini A, Nairn J et al (2011) Cellulose nanomaterials review: structure, properties and nanocomposites. Chem Soc Rev 40:3941–3994

Noonan C, Tajvidi M, Tayeb AH et al (2019) Structure-property relationships in hybrid cellulose nanofibrils/nafion-based ionic polymer-metal composites. Materials (Basel) 12:1269. https://doi.org/10.3390/ma12081269

Österberg M, Vartiainen J, Lucenius J et al (2013) A fast method to produce strong NFC films as a platform for barrier and functional materials. ACS Appl Mater Interfaces 5:4640–4647

Perotti GF, Barud HS, Messaddeq Y et al (2011) Bacterial cellulose–laponite clay nanocomposites. Polymer (Guildf) 52:157–163

Priolo MA, Gamboa D, Holder KM, Grunlan JC (2010) Super gas barrier of transparent polymer–clay multilayer ultrathin films. Nano Lett 10:4970–4974

Rhim J-W, Park H-M, Ha C-S (2013) Bio-nanocomposites for food packaging applications. Prog Polym Sci 38:1629–1652. https://doi.org/10.1016/J.PROGPOLYMSCI.2013.05.008

Segal L, Creely JJ, Martin AE, Conrad CM (1959) An empirical method for estimating the degree of crystallinity of native cellulose using the X-ray diffractometer. Text Res J 29:786–794. https://doi.org/10.1177/004051755902901003

Sehaqui H, Liu A, Zhou Q, Berglund LA (2010) Fast preparation procedure for large, flat cellulose and cellulose/inorganic nanopaper structures. Biomacromolecules 11:2195–2198

Sehaqui H, Morimune S, Nishino T, Berglund LA (2012) Stretchable and strong cellulose nanopaper structures based on polymer-coated nanofiber networks: an alternative to nonwoven porous membranes from electrospinning. Biomacromolecules 13:3661–3667

Sinha Ray S, Bousmina M (2005) Biodegradable polymers and their layered silicate nanocomposites: in greening the 21st century materials world. Prog Mater Sci 50:962–1079. https://doi.org/10.1016/J.PMATSCI.2005.05.002

Siró I, Plackett D (2010) Microfibrillated cellulose and new nanocomposite materials: a review. Cellulose 17:459–494

Spence KL, Venditti RA, Rojas OJ et al (2011) Water vapor barrier properties of coated and filled microfibrillated cellulose composite films. BioResources 6:4370–4388

Tayeb AH, Tajvidi M (2018) Sustainable barrier system via self-assembly of colloidal montmorillonite and cross-linking resins on nanocellulose interfaces. ACS Appl Mater Interfaces 11:1604–1615. https://doi.org/10.1021/acsami.8b16659

Tayeb AH, Latibari AJ, Tajdini A, Sepidehdam SMJ (2012) The influence of pulp refining on de-inking potential and strength properties of ink jet printed paper. BioResources 7:3837–3846

Tayeb AH, Hubbe MA, Tayeb P et al (2017) Soy proteins as a sustainable solution to strengthen recycled paper and reduce deposition of hydrophobic contaminants in paper-making: a bench and pilot-plant study. ACS Sustain Chem Eng 5:7211–7219. https://doi.org/10.1021/acssuschemeng.7b01425

Tayeb AH, Amini E, Ghasemi S, Tajvidi M (2018) Cellulose nanomaterials—binding properties and applications: a review. Molecules 23:2684. https://doi.org/10.3390/molecules23102684

Vilela SO, Soto-Oviedo MA, Albers APF, Faez R (2007) Polyaniline and mineral clay-based conductive composites. Mater Res 10:297–300. https://doi.org/10.1590/S1516-14392007000300015

Wang J, Gardner DJ, Stark NM et al (2018) Moisture and oxygen barrier properties of cellulose nanomaterial-based films. ACS Sustain Chem Eng 6:49–70

Wu CN, Saito T, Fujisawa S et al (2012) Ultrastrong and high gas-barrier nanocellulose/clay-layered composites. Biomacromolecules 13:1927–1932. https://doi.org/10.1021/bm300465d

Yermiyahu Z, Lapides I, Yariv S (2005) Thermo-XRD-analysis of montmorillonite treated with protonated Congo-red. Curve fitting. Appl Clay Sci 30:33–41. https://doi.org/10.1016/J.CLAY.2005.03.002

Yilmaz O, Cheaburu CN, Gülümser G, Vasile C (2012) On the stability and properties of the polyacrylate/Na-MMT nanocomposite obtained by seeded emulsion polymerization. Eur Polym J 48:1683–1695

Zhou Q, Xanthos M (2009) Nanosize and microsize clay effects on the kinetics of the thermal degradation of polylactides. Polym Degrad Stab 94:327–338. https://doi.org/10.1016/J.POLYMDEGRADSTAB.2008.12.009